Influence of Rainfall Infiltration on the Stability of a Residual Soil Slope

Emmanuel Kennedy da Costa Teixeira
Professor, Federal University of São João del-Rey - São João del-Rey, Minas Gerais, Brazil. e-mail: emmanuel.teixeira@ufv.br

Roberto Francisco de Azevedo
Professor, Federal University of Viçosa - Viçosa, Minas Gerais, Brazil. e-mail: razevedo@ufv.br

André Geraldo Cornélio Ribeiro
Professor, Federal University of Lavras - Lavras, Minas Gerais, Brazil - e-mail: andreribeiro@deg.ufla.br

Izabel Christina d'Almeida Duarte de Azevedo
Professor, Federal University of Viçosa - Viçosa, Minas Gerais, Brazil. e-mail: iazevedo@ufv.br

Eduardo Souza Cândido
M. Sc. Student, Federal University of Viçosa - Viçosa, Minas Gerais, Brazil. e-mail: eduardo.candido@ufv.br

ABSTRACT

In tropical countries, like Brazil, many soil slopes are partly or fully composed by non-saturated soils and, in such cases, suction forces increase the shear strength of these materials. When precipitation occurs, part infiltrates and, as the soil layers increase the water content, suction forces decrease, eventually leading the slope to fail. This paper discusses the effect of rainwater infiltration on the safety factor (SF) of a gneiss residual soil slope located at Viçosa Federal University (UFV) campus. The paper presents results of laboratory tests - characterization, direct shear, water retention and permeability curves - performed in disturbed and undisturbed soil samples of different layers identified in the slope by standard penetration tests (SPT). Moreover, it also describes the variations of volumetric water content, suction and SF of the slope along the year of 2011, considering the climatic data measured at UFV weather station. The infiltration analysis was accomplished with the computational program VADOSE/W and the slope stability was calculated daily with the program SLOPE/W, both from GeoStudio 2007 of Geo-Slope International Ltd.. The analysis showed that in dry periods the SF values increased, but with lower rates compared to the decrease rate occurred during rainy periods. The lowest value of the SF was 1.545, in December, which agrees with the stable situation of the slope observed in the field.

KEYWORDS: Slope Stability, Unsaturated Soils, Rainwater Infiltration.

INTRODUCTION

Landslides are a major geologic hazard with estimated tens of deaths and $1–2 billion in economic losses per year in the US. For example, the island of Puerto Rico experiences one or two large events per year, often triggered in steep slope areas by prolonged and heavy rainfall (Lepore et al., 2012). Slope instability due to rainfall is also common in tropical countries as Brazil, often causing economic and human losses (Vargas et al. 1986).

The main causes of slope failures are related to anthropogenic actions, type of soil, and precipitation.

As it is well known, the shear resistance of unsaturated soils increases due to suction effects (Fredlund et al., 1978). During precipitation, part of the water infiltrates in the slope and, as the soil becomes more humid, suction forces reduce, thus causing a decrease in the shear strength that, eventually, leads the slope to fail.

To analyze the influence of rainfall on the stability of a slope it is necessary to know the slope geometry, stratigraphy and the initial water content distribution. Besides, it is also required that water retention and hydraulic conductivity curves, as well as soil shear strength parameters, climate conditions and vegetation (if existent) properties are known.

Available numerical models and instrumented field cases have been helping greatly to better understand the infiltration problems.

Gasmo et al. (2000) studied several slopes and concluded that infiltration of rainwater decreases the stability of the slope. Numerical models were used to study how infiltration into a slope varied with respect to rainfall intensity and to show the effect of infiltration on slope stability through the combined use of seepage and slope stability analyses.

Cho and Lee (2001) calculated the safety factor for an unsaturated slope subjected to a rainfall infiltration using a two-dimensional finite element flow-deformation coupled analysis program. The modified Mohr-Coulomb failure criterion was adopted for the unsaturated soil strength. The analyses of some numerical examples illustrated a typical process of rain-induced infiltration into unsaturated soil slopes and the effect of hydraulic conductivity on slope stability.

Tsaparas et al. (2002) attempted to identify the influence of soil hydrological characteristics and climatic information on the stability of an unsaturated soil slope during rainfall. The numerical analysis showed that the ratio between the saturated coefficient of permeability and the rainfall distribution could significantly influence the seepage pattern within an unsaturated soil slope.

Rahardjo et al. (2005) presented data of an instrumented residual soil slope in Singapore. Results indicated that significant infiltration occurs during rainfalls. Small rainfalls contribute to larger infiltration percentage than large rainfalls. The percentage of infiltration usually decreases with increase total rainfall. The study also indicated a correlation between rainfall amount and relative increase in pore-water pressure.

Chen et al. (2009) analyzed a slope located at the upstream of the Shanher Stream, in Taipei County, that failed on November, 1st 2000, after a heavy rainfall that caused serious disasters in

many areas of northern Taiwan. Laboratory tests and slope stability analysis were performed to obtain the mechanical and hydraulic properties of the soil under unsaturated and saturated conditions. Limit equilibrium method and numerical analysis were utilized to simulate the process of infiltration. The results of the stability analysis showed that the rainfall intensity–time history is the most significant influence factor. The analyzed failure zone and the predicted time the slope failed were comparable to the field observation.

Brunetti et al. (2010) compiled a catalogue listing 753 rainfall events that resulted in landslides in Italy. For each event, the location of the landslide and the time or period of initiation of slope failure are known, together with information on the rainfall duration and mean intensity. A scheme based on four probabilistic thresholds was proposed which could be implemented in landslide warning systems operating on rainfall thresholds, and on precipitation measurements or forecasts.

Ling and Ling (2012) performed a series of centrifuge model simulations with reference to a landslide that occurred during Thyphoon Nabi, Japan, in 2005. The physical model was an infinite sand-clay slope. The results showed that incremental rainfall of less than 200 mm led to local failures, whereas total accumulation of 400 mm resulted in a global failure. A reduction in apparent cohesion combined with an increase in pore-pressure due to infiltration was pointed out as responsible for the slope instability.

Lepore et al. (2012) developed a landslide susceptibility map for Puerto Rico based on two widely applied methodologies: bivariate frequency ratio (FR method) and logistic regression (LR method). This map was tested against previous landslide analyses, demonstrating that the two methods are consistent with landslide susceptibility verified on earlier studies. It turned out to be a robust and verifiable landslide susceptibility map for the whole island of Puerto Rico.

Following these studies, the aim of this paper is to contribute to the discussion on the influence of rainfall infiltration in the safety factor value of a residual soil slope.

MATERIAL AND METHODS

The studied slope is located at the Federal University of Viçosa campus. The slope geometry and stratigraphy were evaluated by means of a topographic survey and two boreholes (SPT - 01 and SPT - 02), respectively.

Disturbed and undisturbed soil samples were collected near the boreholes. Disturbed samples served to determine the grain-size distribution, the Atterberg limits, and the specific weight of the soils particles. Undisturbed samples were used to evaluate the strength parameters, saturated hydraulic conductivity and water retention curves (WRC) of the soils.

The WRC were obtained using both the centrifugal method (Reis et al., 2011), for suction values below 250 kPa, and the filter paper method for higher values of suction. Fredlund and Xing (1994) equation adjusted the WRC obtained experimentally.

The hydraulic conductivity curve was obtained indirectly using the WRC and the saturated hydraulic conductivity. The equation proposed by Fredlund and Xing (1994) was also used to model this curve.

The numerical analysis was performed by using two GeoStudio programs: VADOSE, to evaluate the transient flow in the unsaturated medium considering the atmospheric coupling; and SLOPE/W, to calculate the variation of the slope safety factor during the year of 2011. The choice of this particular year was associated to the failure of an adjacent slope to the studied one, which indeed remained stable.

Stability analyzes were performed using Bishop´s method with unsaturated soil strength parameters calculated through the WRC of the soils (Vanapalli et al. 1996). Minimum safety factors were calculated daily.

Figure 1 presents the cross section of the slope intersecting the two boreholes used in the study. A finite element mesh was established considering the different soils and their respective geotechnical and vegetation parameters (leaf area index, root depth and wilting point). Daily climatic parameters (precipitation, maximum and minimum temperature, wind speed, and maximum and minimum relative air humidity) obtained from Viçosa weather station were used.

PRESENTATION AND ANALYSIS OF RESULTS

Figure 1 shows the stratigraphy of the slope: a layer of sandy silt superimposed on a deeper layer composed almost entirely of fine sand.

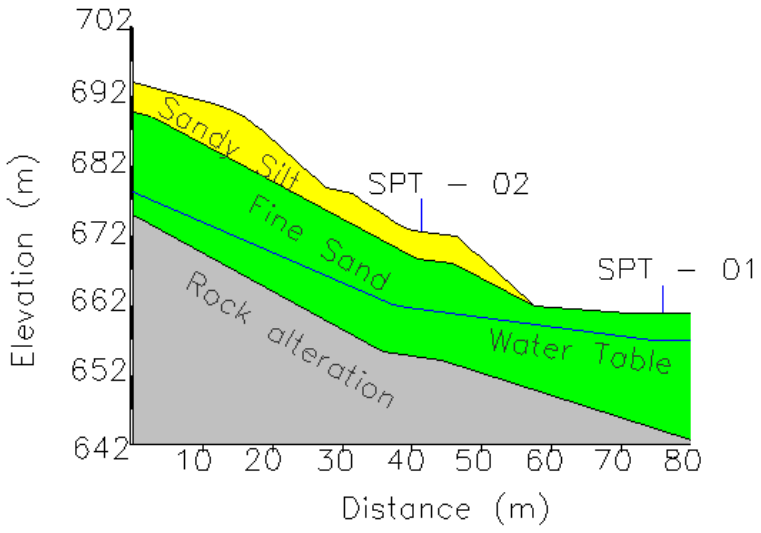

Figure 1: Stratigraphy of the slope and position of the water table for the AA' section.

The soil collected near borehole 1 (SPT - 01) presents 69% of sand, 28% of silt and 3% of clay. Close to borehole 2 (SPT - 02), the soil sample shows 29% of sand, 54% of silt and 17% of clay. According to the Universal Soil Classification System, these two materials are classified, respectively, as SC and MH.

Table 1 presents the parameters of the two soils.

Table 1: Characteristics of the embankment soils.

Soil	Limits			γ_s	k_s
	LL (%)	LP (%)	IP (%)	kN/m^3	cm/s
Fine Sand (SC)	38	21	17	2.706	2.5E^{-4}
Sandy Silt (MH)	59	32	27	3.046	6.8E^{-5}

Table 2 shows effective strength parameters of the soils determined from direct shear tests with saturated and natural samples, using normal stresses of 50, 150 and 300 kPa.

Table 2: Strength parameters of soils SC and MH.

Soil	Condition	γ_{nat} (kN/m^3)	c'(kPa)	ϕ'(°)
SC	Saturated	15.7	15.6	28
	Natural	15.5	50.9	28
MH	Saturated	15.1	44.9	19.4
	Natural	14.6	60.9	34.6

Figures 2 and 3 show the WRC for soil SC and MH, respectively. The minimum error between Fredlund and Xing (1994) curves and the laboratory data was 2.29% (SC) and 2.25% (MH), for the parameters presented in Table 3.

Table 3: Fredlund and Xing (1994) parameters of soils SC and MH.

Soil	Parameters					
	a	n	m	Ψ_r (kPa)	θ_r	θ_s
SC	181.825	2.573	0.776	3.251	0.07	0.417
MH	290.581	5.839	0.514	21.457	0.09	0.536

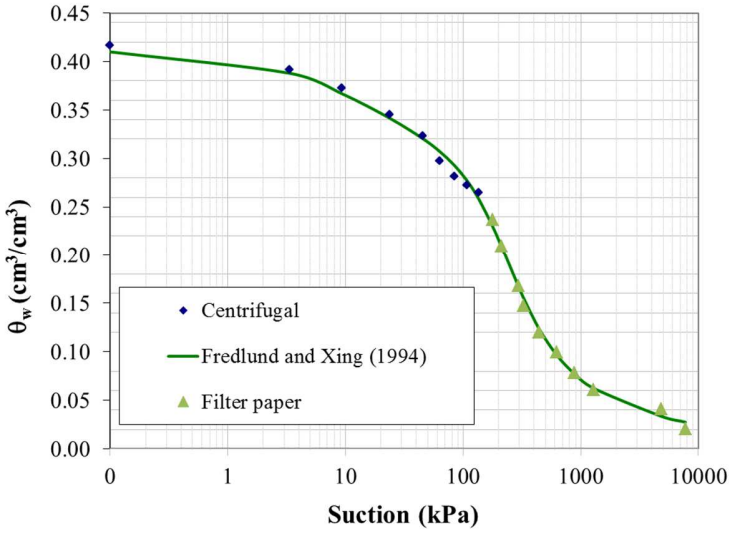

Figure 2: WRC of soil SC.

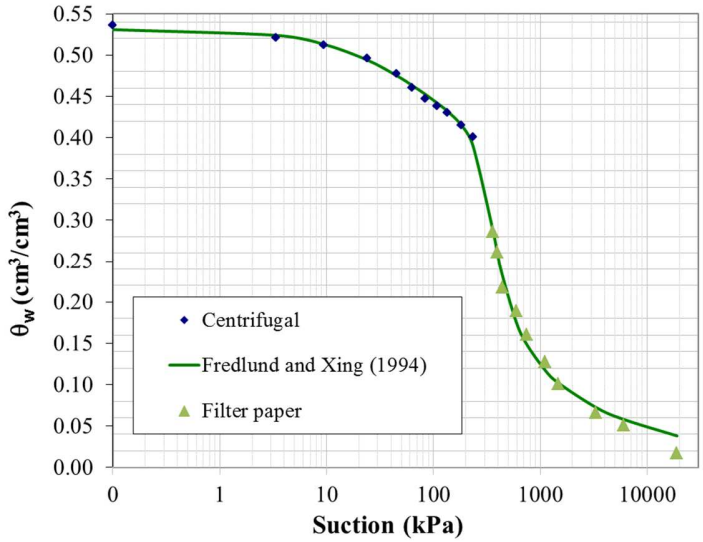

Figure 3: WRC of soil MH.

Figures 4 and 5 present hydraulic conductivity curves for soils SC and MH, respectively, obtained indirectly with parameters of the WRC (Table 3) and the saturated hydraulic conductivities (Table 1), according to the equation proposed by Fredlund and Xing (1994).

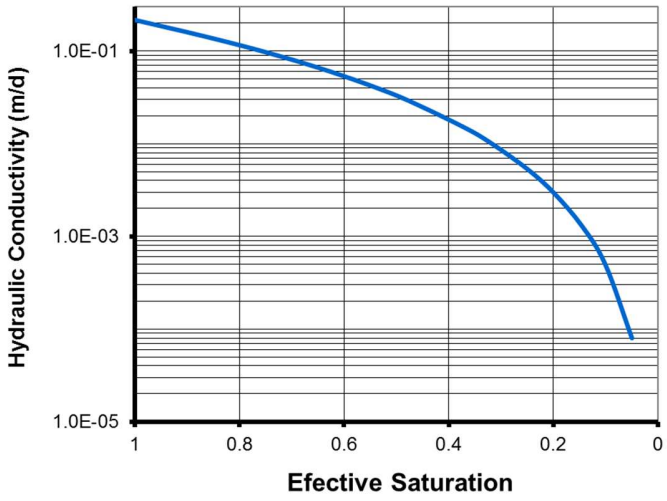

Figure 4: Hydraulic conductivity of soil SC.

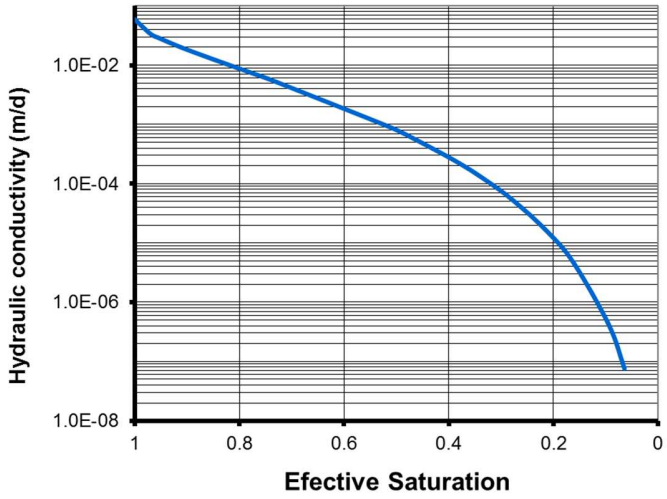

Figure 5: Hydraulic conductivity of soil MH.

Figure 6 shows the finite element mesh used in the numerical model, together with the boundary conditions and the initial water table position. The figure also enhances the nodes were results will be presented.

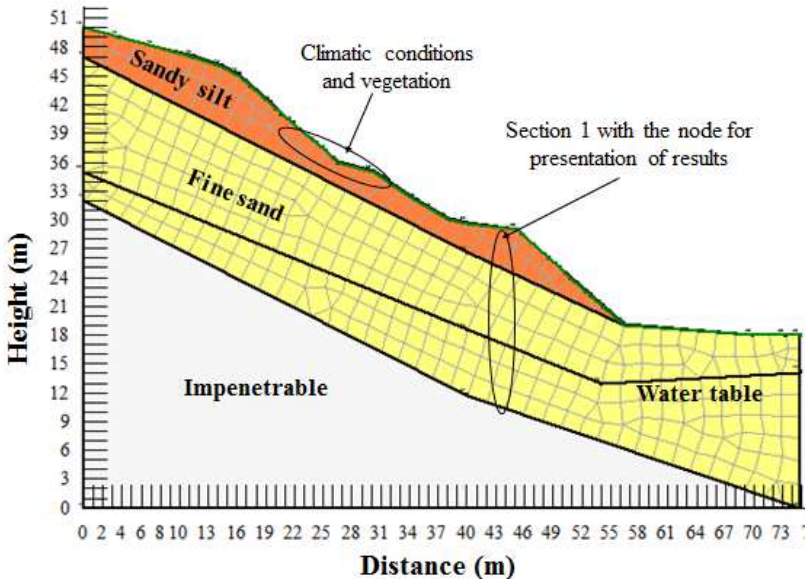

Figure 6: Finite element mesh (491 nodes and 451 elements).

Defined the initial conditions, volumetric water content and suction in all points of the slope, it was performed the transient analysis for the climatic conditions imposed on the slope surface (Figure 7). The volumetric water content and suction were evaluated daily. With the suction values, the minimum safety factor and the corresponding critical failure surface were also calculated daily.

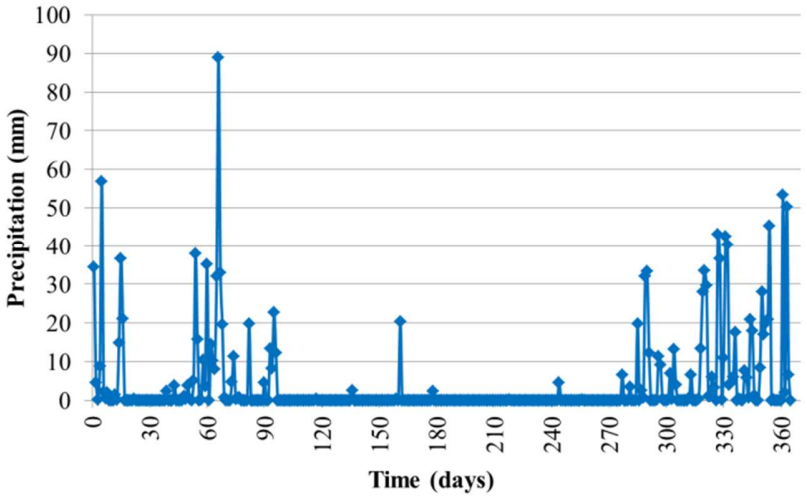

(a)

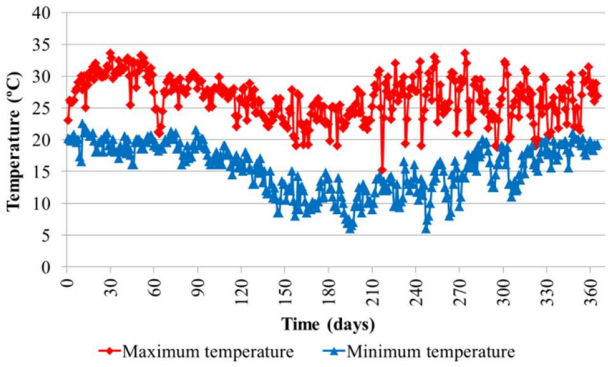

(b)

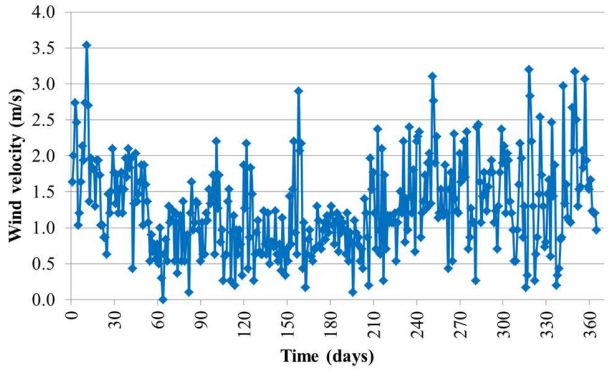

(c)

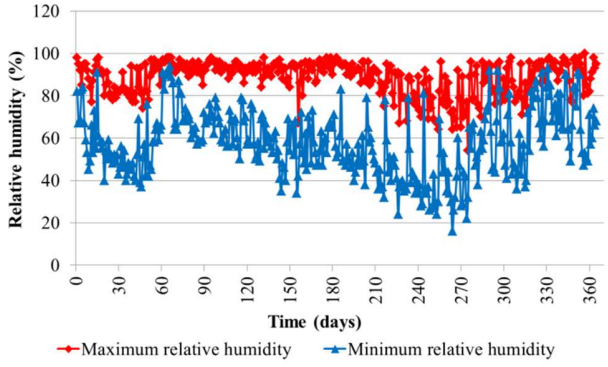

(d)

Figure 7: Viçosa Climate data: (a) precipitation (mm), (b) temperature (oC), (c) wind velocity (m/s) and (d) relative humidity.

Figure 8 presents the volumetric water content variation, in seven different days of the year, at the nodes shown in Figure 6. Day 0 represents the initial condition. Between days 1 and 19, the accumulated rainfall was 183.8 mm. After day 19, there was a short dry period until day 50. Between day 50 and 100, the accumulated precipitation was 414.4 mm. From there on, there was a dry period that extended until day 284. From day 284 to 365, the wettest period of the year, the accumulated rainfall was 782.9 mm.

According to Figure 8, the volumetric water content at the surface points showed values of 0.443, 0.480, 0.434, 0.523, 0.466 and 0.526 cm^3/cm^3, on days 0, 19, 50, 100, 284 and 365, respectively, in accordance to the climatic conditions, as expected.

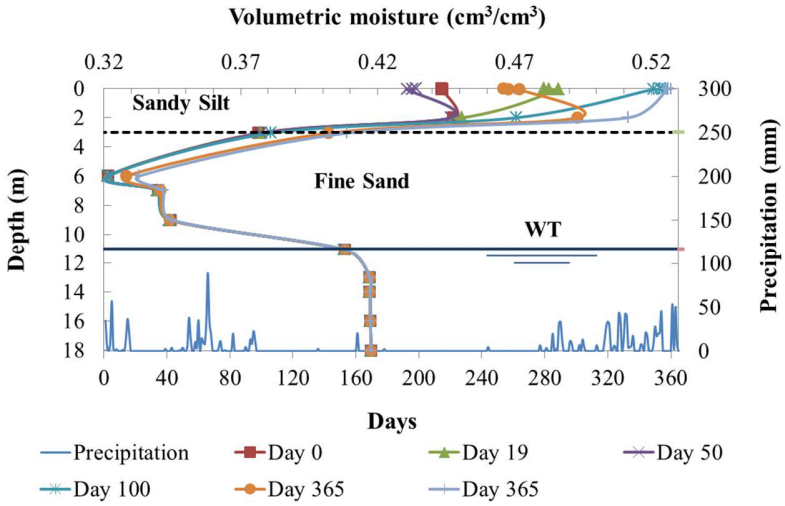

Figure 8: Variation of volumetric water content in seven days throughout the year.

Volumetric water content close to surface oscillated much more than at points deeper than 8.0 m (Figure 8), since the sandy silt layer had a saturated hydraulic conductivity smaller than the one of the layer below (fine sand layer), hindering infiltration into deeper regions. Volumetric water content curves for days 100 and 284 illustrate this assertive. These days correspond to the beginning and the end of the dry season. On day 100, at the surface point on the sandy silt layer, the volumetric water content value was as high as 0.523 cm^3/cm^3. After the dry period, on day 284, that value decreased to approximately 0.466 cm^3/cm^3. The analysis of a point 6.0 m deep in the fine sand layer shows that value of the water content is equal to the initial one (0.32 cm^3/cm^3), in day 100, indicating that the precipitation had not yet reached this point. With more time for infiltration, this value increases to 0.35 cm^3/cm^3, in day 284.

Figure 9 shows values of pore-pressure profiles for days 0, 19, 50, 100, 284 and 365. Again, points closer to the surface present higher variations than the others do. Points located deeper than 9.0 m show no suction variation along the year.

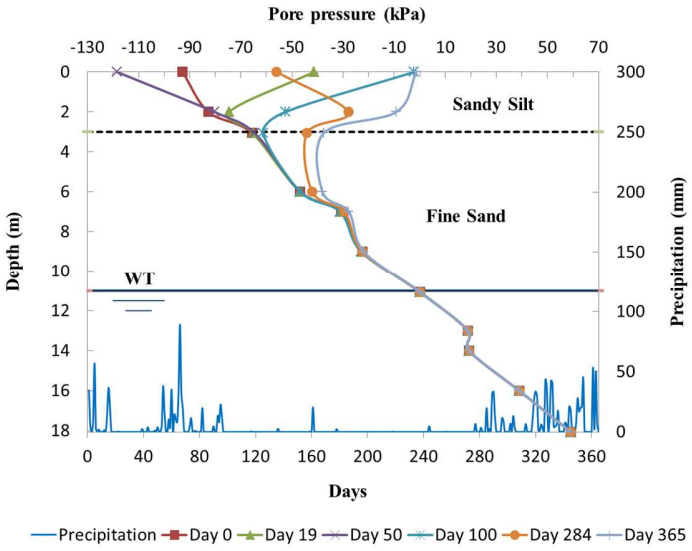

Figure 9: Variation of pore pressure throughout the year.

Figure 10 shows suction variation between days 62 and 70.

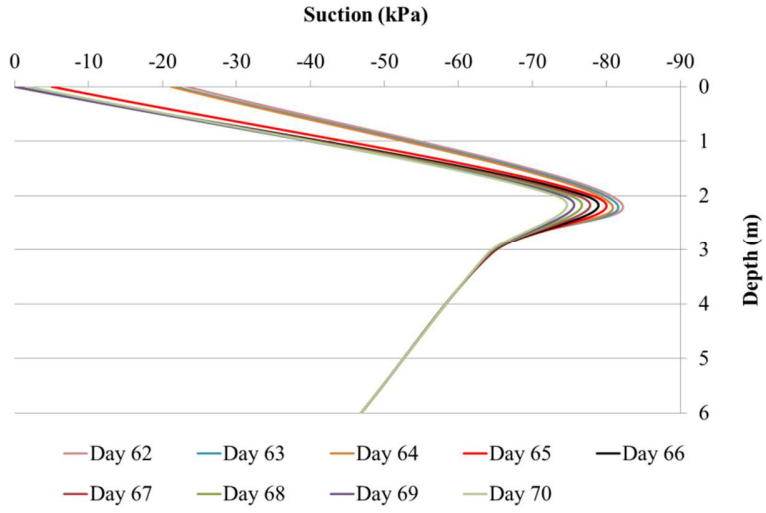

Figure 10: Variation of suction between days 62 and 70.

Precipitation on days 62, 63 and 64 were, respectively, 14.4; 10.3 and 8.0 mm. According to Figure 9, during these days there was no significant variation in the suction profiles and, at the surface, suction value was around 22.0 kPa. On day 65 there was a rainfall of 32.1 mm, causing a significant suction decrease, mainly at the surface, where suction dropped down to around 5.0 kPa.

Zhang et al. (2004) related infiltration with the saturated hydraulic conductivity of the soil, for a constant precipitation value. When precipitation is less than the saturated hydraulic conductivity of the soil, as on days 62, 63 and 64 (Figure 10), a wet infiltration front is formed with soil moisture smaller than the one corresponding to saturation. However, when precipitation is greater than or equal to the saturated hydraulic conductivity of the soil, as on day 66, a saturation front is formed that deepens as a function of the rain duration increase. Suction became equal to zero since the sandy silt soil has a saturated hydraulic conductivity value of 58.7 mm/d, which is smaller than 89.0 mm of precipitation on that day. Thus, results presented in Figure 10 confirm the research of Zhang et al. (2004).

Figure 11 presents slope safety factors along the year of 2011. All values, calculated using Bishop method, correspond to critical slip surfaces. The lowest calculated value of 1.545 correspond to days 354 and 365. The safety factor varied only in the second decimal place, since critical failure surfaces are deeper and go through points where suction varied little during the year.

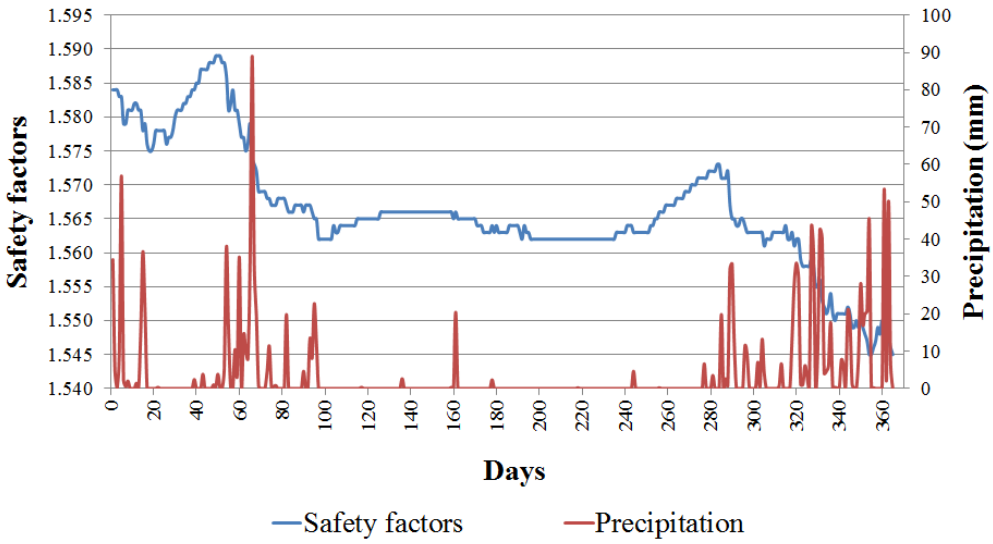

Figure 11: Results of stability analyses along the analyzed period (01/01/2011 to 12/31/2011).

Figure 12 shows factor of safety values for the last days of dry and wet periods of the year 2011.

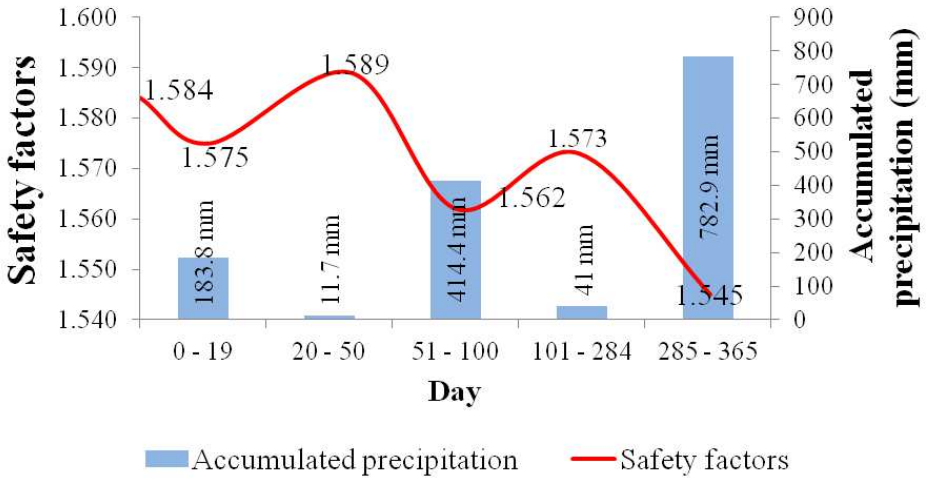

Figure 12: Variation of safety factor according to wet and dry periods throughout the year.

In the first 19 days of the year, the accumulated rainfall was 183.8 mm, which reduced the initial safety factor from 1.584 to 1.575. Between days 20 and 50, cumulative rainfall was only 11.7 mm, raising the SF to 1.589. A new rainy period totalizing 414.4 mm occurred up to the day 100, which lowered the safety factor to 1.562. Subsequently, there was a long dry period of about six months during which the accumulated precipitation was only 41 mm. Consequently, SF rose to 1.573. However, during this period SF values stayed most of the time between 1.563 and 1.564 (Figure 11), increasing more significantly only in the last 20 days. Safety factor increase after rain stop occurred in a smaller rate than its reduction in the beginning of rainy season (Fredlund and Rahardjo, 1993). After day 284, the wettest period of the year started, totalizing 782.9 mm, and SF reached its lowest value, 1.545.

Since points near the surface are more susceptible to precipitation, they suffer greater variations of volumetric water content and suction, and influence more directly the safety factor (Figure 13). Between day 0 and 19, the infiltration front advances, increasing the water content, reducing suction, and consequently the value of the safety factor. During the dry period, between days 100 and 284, it happens the other way around.

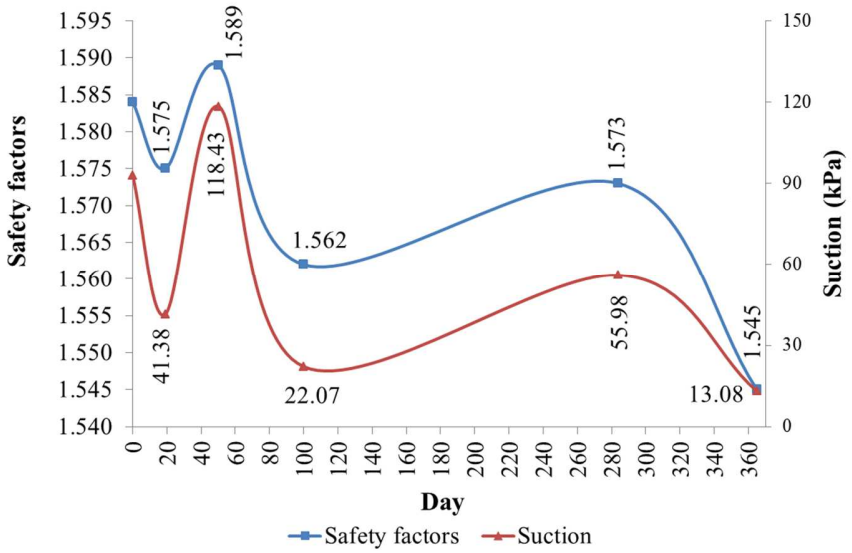

Figure 13: Relationship between the variation of the safety factor and the suction throughout the year.

The most critical slip surface along the year is shown in Figure 14. The corresponding safety factor is 1.55, indicating that the slope was stable throughout the year, as it was really observed.

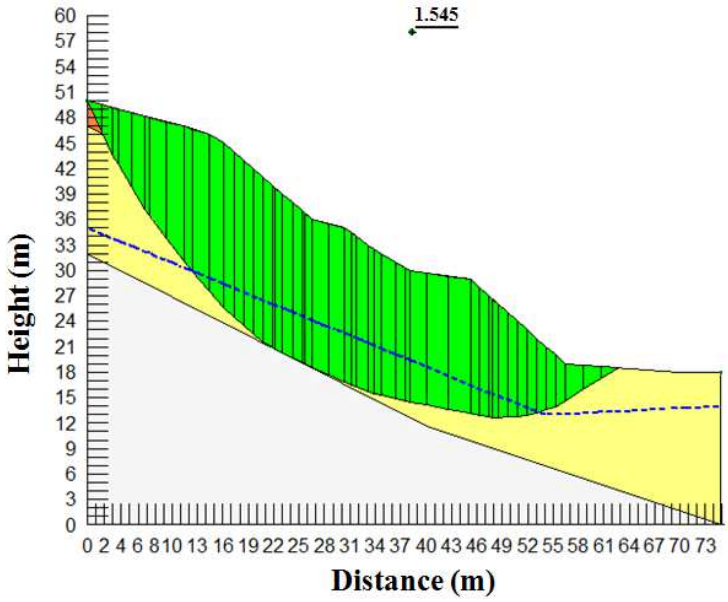

Figure 14: Results of the slope stability analysis of the most critical day in 2011.

CONCLUSION

The stability of a slope made of two residual soils, a superficial fine silt sandy layer over a thick fine sand layer, was studied in this paper. The saturated hydraulic conductivity of the silt sandy was lower than the one of the fine sand, which led to a decrease of rainwater infiltration and to an increase of runoff.

Strength parameters of the two soils were obtained from direct shear tests in natural and saturated samples. Cohesion of both soils was greater in natural than in saturated conditions. The friction angle for the sandy silt soil did not vary as expected, although this parameter for MH soil was higher in natural condition.

Water retention curves were obtained using a small centrifuge for lower suction values and with the filter paper method for higher suctions values. The results from both methods agreed and were well adjusted using Fredlund and Xing (1994) equation. Errors of 2.9% for the fine sand and 2.25% for the sandy silt were observed.

Water balance was modeled to analyze the effect of weather conditions on the variation of water content and suction in the slope. At points located near the surface, it was observed greater variation in volumetric water content than at those deeper. For the slope section analyzed, points deeper than 7.0 m indicated no moisture variation during the year, which is attributed to a lower value of the surface layer saturated hydraulic conductivity compared to that of the underlying layer. The longer the duration and higher the intensity of precipitation are, the lower the values of safety factors. This is due to the increase of the volumetric water content and the decrease of suction, which reduces the resistance of the slope.

During the analyzed year, the studied slope presented a small variation in the values of safety factors since there were only little suction variations at shallow points of the slope.

During the dry season, the safety factor variation was smaller than during the rainy period.

The lowest safety factor value was 1.545 on days 354 and 365, justifying the stability of studied slope.

ACKNOWLEDGEMENTS

The authors thank CAPES for the MSc. scholarship granted to the first author and to Federal University of Viçosa for giving the support that made this work possible.

REFERENCES

1. Brunetti, M. T., Peruccacci, S., Rossi, M., Luciani, S., Valigi, D., & Guzzetti, F. (2010). Rainfall thresholds for the possible occurrence of landslides in Italy. Natural Hazards and Earth System Science, 10(3), 447-458.

2. Chen, R. H., Chen, H. P., Chen, K. S., & Zhung, H. B. (2009). Simulation of a slope failure induced by rainfall infiltration. Environmental geology, 58(5), 943-952.
3. Cho, S. E., & Lee, S. R. (2001). Instability of unsaturated soil slopes due to infiltration. Computers and Geotechnics, 28(3), 185-208.
4. Fredlund, D. G., Morgenstern, N. R., & Widger, R. A. (1978). The shear strength of unsaturated soils. Canadian geotechnical journal, 15(3), 313-321.
5. Fredlund, D. G.; Rahardjo, H. (1993). Soil Mechanics for Unsaturated Soils. New York: John Wiley & Sons, 517p.
6. Fredlund, D. G., & Xing, A. (1994). Equations for the soil-water characteristic curve. Canadian geotechnical journal, 31(4), 521-532.
7. Gasmo, J. M., Rahardjo, H., & Leong, E. C. (2000). Infiltration effects on stability of a residual soil slope. Computers and Geotechnics, 26(2), 145-165.
8. Lepore, C., Kamal, S. A., Shanahan, P., & Bras, R. L. (2012). Rainfall-induced landslide susceptibility zonation of Puerto Rico. Environmental Earth Sciences, 66(6), 1667-1681.
9. Ling, H., & Ling, H. I. (2012). Centrifuge model simulations of rainfall-induced slope instability. Journal of geotechnical and geoenvironmental engineering, 138(9), 1151-1157.
10. Martins Reis, R., Nogueira Sterck, W., Bastos Ribeiro, A., Dell'Avanzi, E., Saboya, F., Tibana, S., Marciano, C. R., & Ramires Sobrinho, R. (2011). Determination of the Soil-Water Retention Curve and the Hydraulic Conductivity Function Using a Small Centrifuge. ASTM geotechnical testing journal, 34(5), 457-466.
11. Rahardjo, H., Lee, T. T., Leong, E. C., & Rezaur, R. B. (2005). Response of a residual soil slope to rainfall. Canadian Geotechnical Journal, 42(2), 340-351.
12. Tsaparas, I., Rahardjo, H., Toll, D. G., & Leong, E. C. (2002). Controlling parameters for rainfall-induced landslides. Computers and Geotechnics, 29(1), 1-27.
13. Vanapalli, S. K., Fredlund, D. G., Pufahl, D. E., & Clifton, A. W. (1996). Model for the prediction of shear strength with respect to soil suction. Canadian Geotechnical Journal, 33(3), 379-392.
14. Vargas Jr, E., Oliveira, A. R. B., Costa Filho, L. M., & Campos, T. P. (1986). A study of the relationship between the stability of slopes in residual soils and rain intensity. In International Symposium on Environmental Geotechnology. Envo Publishing, Leigh, USA (pp. 491-500).
15. Zhang, L. L., Fredlund, D. G., Zhang, L. M., & Tang, W. H. (2004). Numerical study of soil conditions under which matric suction can be maintained. Canadian Geotechnical Journal, 41(4), 569-582.